

The first observation of an intermediate flare from SGR 1935+2154

A. V. Kozlova^{1*}, G. L. Israel², D. S. Svinkin¹, D. D. Frederiks¹, V. D. Pal'shin¹,
A. E. Tsvetkova¹, K. Hurley³, J. Goldsten⁴, D. V. Golovin⁵, I. G. Mitrofanov⁵ and
X.-L. Zhang⁶

¹*Ioffe Institute, Politekhnicheskaya 26, St. Petersburg 194021, Russia*

²*INAF - Astronomical Observatory of Rome, Monte Porzio Catone (RM), I-00078, Italy*

³*Space Sciences Laboratory, University of California, 7 Gauss Way, Berkeley, CA 94720-7450, USA*

⁴*Applied Physics Laboratory, Johns Hopkins University, Laurel, MD 20723, U.S.A.*

⁵*Space Research Institute, 84/32, Profsoyuznaya, Moscow 117997, Russia*

⁶*Max-Planck-Institut für extraterrestrische Physik, Giessenbachstrasse 1, D-85748 Garching, Germany*

Accepted 2016 May 8; Received 2016 May 8; in original form 2015 December 23

ABSTRACT

We report on the bright burst detected by four Interplanetary network (IPN) spacecraft on 2015 April 12. The IPN localization of the source is consistent with the position of the recently discovered soft gamma-repeater SGR 1935+2154. From the Konus-*Wind* (KW) observation, we derive temporal and spectral parameters of the emission, and the burst energetics. The rather long duration of the burst (~ 1.7 s) and the large measured energy fluence ($\sim 2.5 \times 10^{-5}$ erg cm⁻²) put it in the class of rare “intermediate” SGR flares, and this is the first one observed from SGR 1935+2154. A search for quasi-periodic oscillations in the KW light curve yields no statistically significant signal. Of four spectral models tested, optically thin thermal bremsstrahlung and a single blackbody (BB) function can be rejected on statistical grounds; two more complex models, a cutoff power law (CPL) and a sum of two BB functions (2BB), fit the burst spectra well and neither of them may be ruled out by the KW observation. The CPL and 2BB model parameters we report for this bright flare are typical of SGRs; they are also consistent with those obtained from observations of much weaker and shorter SGR 1935+2154 bursts with other instruments. From the distribution of double blackbody spectral fit parameters we estimate the SGR 1935+2154 distance to be < 10.0 kpc, in agreement with that of the Galactic supernova remnant G57.2+0.8 at 9.1 kpc.

Key words: pulsars: individual: SGR 1935+2154 – stars: magnetars – gamma-rays: stars

1 INTRODUCTION

The history of observations of Soft Gamma Repeaters (SGRs) began over 30 years ago. The sources were discovered through the detection of recurrent short (~ 0.1 s) bursts of hard X-rays/soft γ -rays by the Konus instrument aboard the Venera 11-14 spacecraft. The first bursts were initially classified as a subtype of gamma-ray bursts (GRB), one with a short duration and a soft spectrum (Mazets & Golenetskii 1981). Now the SGRs are believed to be one of two observational manifestations of “magnetars”, isolated neutron stars (NSs) in which the dominant source of free energy is their

intense magnetic field ($B \sim 10^{14} - 10^{15}$ G) (see Mereghetti 2013 for a detailed review and Olausen & Kaspi 2014 for a recent catalog).

Today we know that the numerous short bursts, with a total energy release E_{tot} of $\sim 10^{38} - 10^{40}$ erg, are the most common manifestation of the SGR bursting activity, but there are two other, rarer types of bursts emitted by SGRs: giant and intermediate flares. The extraordinary giant flares (GFs) are the most intense Galactic events (Hurley et al. 2005). So far, only three GFs have been observed from three out of 23 confirmed magnetars. They display an extremely bright, short, hard initial pulse having a huge $E_{\text{tot}} \sim 10^{44} - 10^{46}$ erg followed by a long-duration decaying tail modulated with the NS rotation period. Quasi-periodic oscillations (QPOs)

* E-mail: ann_kozlova@mail.ioffe.ru

discovered in the GFs of SGR 1806-20 and SGR 1900+14 (Israel et al. 2005; Strohmayer & Watts 2005) and, more recently in short bursts (Huppenkothen et al. 2014a,b) are expected to help us study the properties of matter in NSs. Through detection of the frequencies of NS oscillations, it might be possible to deduce neutron star masses and radii, the equation of state, and other physical properties (e.g., Doneva et al. 2013; Andersson & Kokkotas 1996). The high-fluence intermediate flares (IFs, Olive et al. 2004) last from a few seconds up to a few tens of seconds; the brightest of them have $E_{\text{tot}} \geq 10^{42}$ erg and the peak luminosity reaches $L_{\text{peak}} \geq 10^{43}$ erg s $^{-1}$ (Mazets et al. 1999b; Feroci et al. 2003; Mereghetti et al. 2009; Göğüş et al. 2011), less than that of GFs, though orders of magnitude larger than that of the bulk of the SGR burst population. Although the first observed IFs date back to the early 1980's (Golenetskii et al. 1984; Aptekar et al. 2001), only a few dozen flares have been detected so far and the properties of such outstanding events are of special interest.

The source discussed here, SGR 1935+2154, was discovered on 2014 July 5 through a series of three short bursts (Stamatikos et al. 2014; Lien et al. 2014), detected by the *Swift*/Burst Alert Telescope (BAT). Several days later, its persistent pulsating X-ray counterpart was discovered by the *Chandra* X-ray Observatory (Israel et al. 2014) with a pulse period of ~ 3.2 s. The location of the SGR as determined by the *Swift*/X-ray Telescope (XRT) (Cummmings et al. 2014) lies very close to the geometric centre of the Galactic supernova remnant (SNR) G57.2+0.8 (Gaensler 2014), whose distance is estimated to be 9.1 kpc (Pavlović et al. 2013). In 2015 February the *Fermi*/Gamma-ray Burst Monitor (GBM) and BAT observed weak burst activity from the source – the first one since the discovery.

In this paper, we report on the first observed IF from SGR 1935+2154, which was detected by four Interplanetary network (IPN) spacecraft on 2015 April 12. In Section 2, we describe the IPN triangulation and localization of the burst. In Section 3, we present the results of temporal and spectral analyses of the Konus-*Wind* (KW) data. We describe the search for QPOs in the KW light curve in Section 4. Finally, we compare our results to those obtained previously for short bursts and IFs from known SGRs and discuss the SGR 1935+2154 distance estimate based on the distribution of double blackbody spectral fit parameters. Unless otherwise specified, all errors refer to 1σ confidence limits.

2 IPN LOCALIZATION

On 2015 April 12, a bright, SGR-like burst was detected by four IPN experiments – *INTEGRAL* SPI-ACS (Rau et al. 2005), in a highly elliptical orbit, Konus-*Wind* (Aptekar et al. 1995), in orbit around the Lagrangian point L1, *MESSENGER* GRNS (Gold et al. 2001), in orbit around Mercury, and *Mars-Odyssey* HEND (Hurley et al. 2006), in orbit around Mars – at 0.28, 5.6, 659.6, and 1200.1 light-seconds from Earth, respectively.

An initial 1118 sq. arcmin IPN error box (Golenetskii et al. 2015) was derived using KW, *INTEGRAL*, and *Odyssey*. Later, with *MESSENGER* added, the source was triangulated to a smaller 280 sq. arcmin IPN error box which is inside the initial box. The final

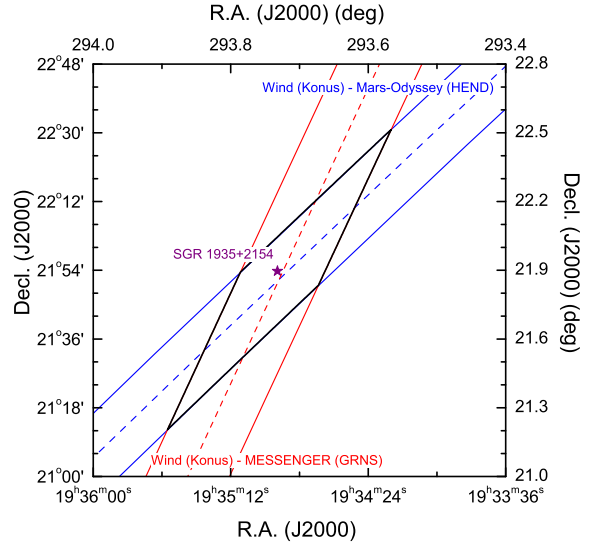


Figure 1. Final, 280 sq. arcmin IPN error box of 2015 April 12 burst, defined by the 7:08 wide *Wind-Odyssey* and 6:72 wide *Wind-MESSENGER* annuli. The position of SGR 1935+2154 is indicated by the star.

box is centered at R.A.(J2000) = 19^h34^m55^s, decl.(J2000) = +21°51'49" and its maximum dimension is 1:34 (the minimum one is 6:72). The position of SGR 1935+2154 (Cummmings et al. 2014) lies inside the final error box, 1:97 from its centre (Fig. 1).

3 KONUS-WIND OBSERVATION

The burst triggered KW at $T_0 = 41064.683$ s UT (11:24:24.683) on 2015 April 12. The propagation delay from *Wind* to Earth is 1.361 s for this burst; correcting for this factor, the KW trigger time corresponds to the Earth-crossing time 41066.044 s UT (11:24:26.044).

3.1 Time history

The event time histories were recorded in three energy bands: G1 (20–80 keV), G2 (80–300 keV) and G3 (300–1200 keV) with a time resolution of 2 ms from $T_0 - 0.512$ s to $T_0 + 0.512$ s and 16 ms afterwards. The burst light curves in bands G1 and G2 (Fig. 2) show a single, very bright pulse which starts at $\sim T_0 - 0.062$ s with a sharp (<10 ms) rise, peaks at $\sim T_0 + 0.800$ s and decays to background level at $\sim T_0 + 1.680$ s. KW observed no statistically significant emission above ~ 300 keV (the G3 band), which, accounting for the burst brightness, suggests a soft energy spectrum. The total burst duration $T_{100} = 1.742$ s was determined at the 5σ level in the G1+G2 energy band (20–300 keV). The corresponding values of T_{90} and T_{50} are 1.412 ± 0.016 and 0.654 ± 0.016 s, respectively.

While the KW count rate in this burst reaches $\sim 5 \times 10^4$ counts s $^{-1}$, it does not exceed $\sim 15\%$ of the saturation level, which makes the standard KW dead time (DT) correction procedure reliable (the procedure uses a

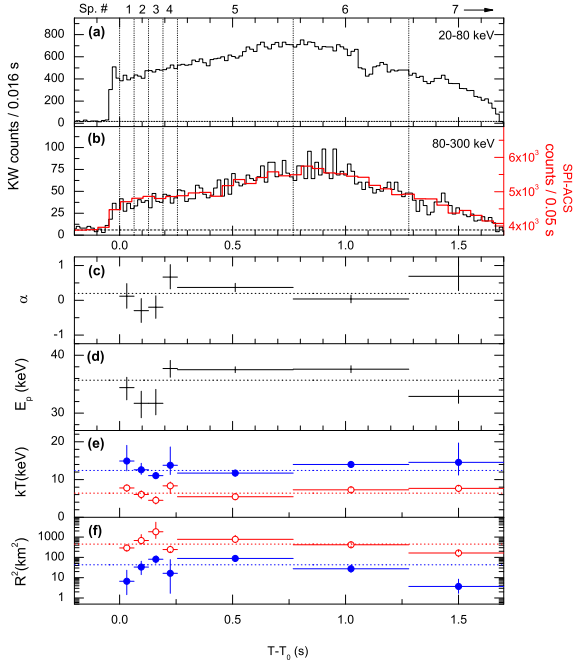


Figure 2. Light curves of the burst recorded by *Konus-Wind* in the G1 (20–80 keV, panel (a)) and G2 (80–300 keV; panel (b), black line) energy ranges with 16 ms resolution; the *INTEGRAL* SPI-ACS light curve ($\gtrsim 80$ keV, 50 ms resolution) is shown with a red line in panel (b). The vertical dotted lines denote the intervals over which the KW spectra were accumulated; the right boundary of spectrum 7 ($T_0 + 9.472$ s) is not shown. The KW count rates are dead-time corrected and the horizontal dashed lines indicate the background levels. The *INTEGRAL* time scale is corrected for the burst propagation between the spacecraft. Time-resolved CPL and 2BB fit parameters are given in panels (c) to (f); low- and high- kT components of 2BB are shown by open and filled symbols, respectively; the horizontal dotted lines indicate the value of the parameters measured for the time-integrated spectrum.

non-paralyzable correction with a DT of 2–5 microseconds, depending on the energy band; details of the KW DT corrections at high count rates can be found in Mazets et al. (1999a). Given the soft energy spectrum, the DT-corrected KW light curve in the G2 band (80–300 keV) can be directly compared to the SPI-ACS data ($E \gtrsim 80$ keV). At the SPI-ACS count rate of $\sim 1.1 \times 10^5$ counts s^{-1} observed in this burst the DT effects are negligible (Mereghetti et al. 2005); and a clear similarity in the shapes of the two instrument light curves (panel (b) in Fig. 2) demonstrates the correctness of our analysis.

3.2 Spectral analysis and the burst energetics

During the burst, the instrument measured seven multichannel energy spectra covering a wide energy range from 20 keV to 14 MeV; the accumulation times are given in Tab. 1. For the spectral fits, we use only the 20 to 250 keV energy interval since no emission was detected at higher energies. At high count rates a pile-up effect in the analog electronics can distort the low-energy part of the KW instrumental spectra (e.g., Frederiks et al. 2013). Our previous sim-

ulations show that for events with soft, SGR-like incident spectra and count rates similar to those in this event, the scale of the resulting distortion does not exceed statistical errors in the corresponding spectral channels. Accordingly, spectral fits we made to the simulated data did not reveal a statistically significant difference between the model and the best-fit spectral parameters. Thus our analysis of the SGR 1935+2154 burst spectra relies on standard fitting procedures with no special precautions due to high count rates being taken.

The spectral analysis was performed in XSPEC, version 12.8 (Arnaud 1996), by applying two spectral models, which have been shown to be the best-fits to the broadband spectra of SGR bursts (e.g. Feroci et al. 2004; Olive et al. 2004; Lin et al. 2012; van der Horst et al. 2012). The first one is a sum of two blackbody functions with the normalization proportional to the surface area (2BB). The second model is a power law with an exponential cutoff (CPL), parametrized as $E_p: f(E) \propto E^\alpha \exp(-(2 + \alpha)E/E_p)$, where α is the power-law photon index and E_p is the peak energy in the νF_ν spectrum. We also tried to fit the spectra to a single blackbody (BB) function and to an optically thin thermal bremsstrahlung (OTTB, $f(E) \propto E^{-1} \exp(-E/kT_{\text{OTTB}})$) and found that both models may be rejected on statistical grounds.

A summary of the KW spectral fits with 2BB and CPL models is presented in Tab. 1. Two methods were used to obtain the best-fit parameters for any given spectral model. In the first method, the raw count rate spectra were rebinned in order to have at least 10 counts per energy bin, and fitted using χ^2 minimization. The alternative method uses the Castor C-statistic (C-stat) minimization and the spectra rebinned to have a minimum of one count per bin. For spectra 1-4, with the short accumulation times and poor count statistics in higher energy channels, the fits using C-stat gave smaller uncertainties in the parameters than those using the χ^2 statistic, but they are consistent with each other within the uncertainties. In these cases we report the results obtained with the C-statistic and provide a quality of the corresponding χ^2 fit for reference. Otherwise, the results obtained with χ^2 are provided. We note that spectrum 7 was measured from $T_0 + 1.280$ s to $T_0 + 9.472$ s and no burst emission was detected after $T_0 + 1.680$ s. For this spectrum, BB radii and the corresponding luminosities obtained from the XSPEC fits were re-calculated using the accumulation interval 1.280–1.680 s; accordingly, for the time-integrated spectrum the BB normalizations are given for the interval 0.0–1.680 s.

Both CPL and 2BB models fit the time-integrated (TI) spectrum (Fig. 3) and all seven time-resolved (TR) spectra well, with $\chi^2/\text{dof} = 1.23$ (30 dof) in the worst case and a null hypothesis probability of > 0.18 for all fits. When comparing the fit statistic for individual spectra, the difference between CPL and 2BB fits, $\Delta\chi^2_{\text{CPL-2BB}}$, lies between -5.4 and $+2.7$ with nearly equal numbers of positive and negative values of $\Delta\chi^2_{\text{CPL-2BB}}$ obtained (the behaviour of C-stat is very similar and, hereafter, we focus on the χ^2 statistic only).

Since these two models are not nested, the most preferred model can not be chosen based on a test statistic (TS) with known reference distribution (e.g., using an F -test or a likelihood ratio test). This difficulty can be overcome e.g. by employing a Bayesian approach when a posterior predictive

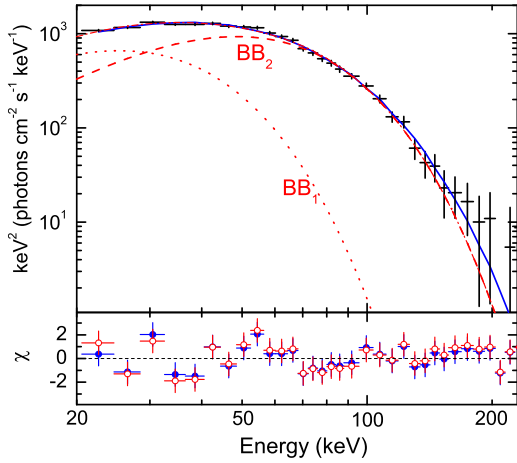


Figure 3. Time-integrated νF_ν spectrum of the flare: KW data (symbols); the CPL model (blue solid line); the 2BB model (red dashed-dotted line) and its low- kT and high- kT components (red dotted and dashed lines, respectively). The bottom panel shows the fit residuals: filled and open symbols represent CPL and 2BB, respectively.

distribution of an arbitrary TS is created via Monte Carlo simulations of the model parameters. Following the recipe from Protassov et al. (2002), we ran a set of simulations in XSPEC in order to evaluate the capability of KW to distinguish between the two models for the SGR 1935+2154 spectra. For each of the time intervals we simulated two sets of 1000 spectra using CPL or 2BB as a null model and fitted the simulated spectra with both models. From the fits, we built posterior predictive distributions of $\Delta\chi^2$ and calculated the posterior predictive p -values. The latter represent, in our case, the probability for an incident CPL (2BB) spectrum to be fit by 2BB (CPL) model with more extreme $\Delta\chi^2$ than that obtained from the real spectrum. For none of the time intervals did we find $p < 10^{-2}$. CPL can be preferred to 2BB ($p \lesssim 0.05$) only for spectrum #6 ($p = 0.051$) and for the TI spectrum ($p = 0.019$), while 2BB cannot be favoured at a level better than $p = 0.173$ achieved for spectrum #1. Proceeding from this, and from the good agreement found for both spectral functions with the measured data, we conclude that neither CPL nor 2BB may be ruled out by the KW observations and consider below the results obtained with both models.

The TI spectrum 1-7 is well fitted by the CPL model ($\chi^2 = 32.4/31$ dof) with α of $\simeq 0.20$ and $E_p \simeq 35.7$ keV. The time-resolved spectral parameters are plotted in panels (c–f) in Fig. 2. The TR peak energies of the CPL model in individual spectra range from ~ 31.7 to ~ 37.5 keV, with a slight correlation to the energy flux. The photon index shows more prominent variation: α changes over a wide range of hard values, between -0.3 and $+0.7$, showing no apparent dependence on the emission intensity.

The 2BB model applied to the TI spectrum also yields a reasonably good fit ($\chi^2 = 37.0/30$ dof). The temperatures of the soft and hard BB components are $kT_1 \simeq 6.4$ and

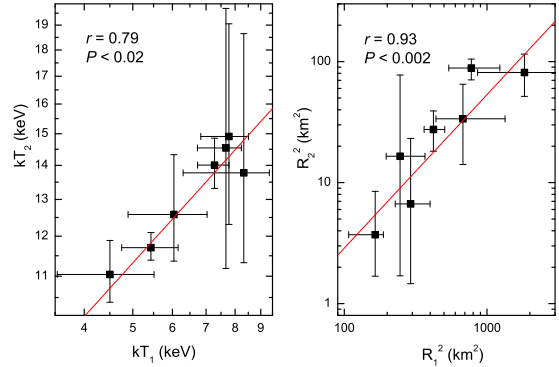


Figure 4. Correlations between the cool and hot blackbody parameters: temperatures (left panel) and emission areas (right panel). Spearman-rank correlation coefficients r and chance probabilities P are indicated in each panel. Solid lines represent the best-fit power-law approximations (see text).

$kT_2 \simeq 12.4$ keV, and the corresponding radii of the emitting areas (calculated at a distance of 10 kpc) are $R_1 \simeq 21.3$ and $R_2 \simeq 6.6$ km, respectively.

The TR kT_1 values vary in the ~ 4.5 – 8.5 keV range. Although kT_2 has large uncertainties in some spectra, the best-fit values are located between 11 and 15 keV and show smaller relative fluctuations than kT_1 , with $\sigma(\log kT_2) = 0.050$ as compared to $\sigma(\log kT_1) = 0.098$. Finally, the TR BB radii as well as the derived BB luminosities generally follow the count rate evolution. A simple statistical test suggests that the fluctuations observed in the CPL and 2BB model parameters can hardly be interpreted as purely statistical; fits with a constant level lead to $\chi^2 > 11.2/6$ dof for all the spectral parameters, indicating that some spectral variability is present over the duration of the burst.

Fig. 4 shows a correlation between the cool and hot BB temperatures derived for individual spectra (left panel), as well as between the time-resolved BB emission areas (right panel). Spearman-rank correlation coefficients r and chance probabilities P are indicated in each panel. While the emission area correlation, with $r = 0.93$, is almost significant at the $>3\sigma$ level, the temperatures are less strongly correlated. When fitted by a power law, the slopes of the correlations are 0.52 ± 0.14 and 1.27 ± 0.17 for the temperatures and the radii, respectively. Finally, the blackbody radii are anti-correlated with corresponding BB temperatures (see Fig. 6 and discussion below).

From the CPL spectral fits, we estimate the total energy fluence of the burst S to be $(2.50 \pm 0.03) \times 10^{-5}$ erg cm^{-2} and the peak energy flux F_{max} to be $(2.15 \pm 0.13) \times 10^{-5}$ erg $\text{cm}^{-2} \text{s}^{-1}$ in a 16 ms time interval starting at $T_0 + 0.800$ s; both values are calculated in the 20–200 keV energy range. From the 2BB fits, the bolometric fluence and peak flux estimates are $\sim 3.3 \times 10^{-5}$ erg cm^{-2} and $\sim 3.0 \times 10^{-5}$ erg $\text{cm}^{-2} \text{s}^{-1}$, respectively. The low- kT BB component contributes about 27 per cent to the total 20–200 keV flux and about 42 per cent to the total bolometric fluence.

Table 1. Spectral fits with 2BB and CPL models.

Spectrum	Interval (s from T_0)	kT_1 (keV)	Norm_1 R_{km}^2/d_{10}^2	L_1^a (10^{39} erg)	2BB Model			χ^2/dof^b	α	CPL Model	
					kT_2 (keV)	Norm_2 R_{km}^2/d_{10}^2	L_2^a (10^{39} erg)			E_{peak} (keV)	χ^2/dof^b
1	0.0 - 0.064	$7.8^{+0.7}_{-0.9}$	292^{+107}_{-64}	137^{+22}_{-33}	$14.9^{+4.1}_{-2.6}$	$6.7^{+16.6}_{-5.2}$	49.0^{+34}_{-23}	11.9/25 [4.8/15]	$0.12^{+0.36}_{-0.35}$	$34.4^{+1.8}_{-2.1}$	14.5/26 [6.9/16]
2	0.064 - 0.128	$6.0^{+1.0}_{-1.1}$	678^{+660}_{-239}	116^{+29}_{-27}	$12.6^{+1.8}_{-1.2}$	$33.7^{+31.3}_{-19.6}$	108^{+33}_{-37}	10.5/21 [8.3/15]	$-0.30^{+0.35}_{-0.34}$	$31.7^{+2.1}_{-2.5}$	10.3/22 [8.1/16]
3	0.128 - 0.192	$4.5^{+1.0}_{-1.0}$	1830^{+3650}_{-970}	96^{+20}_{-19}	$11.0^{+0.9}_{-0.7}$	$81.3^{+34.0}_{-26.7}$	155^{+20}_{-25}	26.7/24 [15.0/15]	$-0.20^{+0.33}_{-0.32}$	$31.7^{+2.4}_{-2.0}$	28.3/25 [16.4/16]
4	0.192 - 0.256	$8.5^{+1.0}_{-2.0}$	246^{+122}_{-49}	151^{+50}_{-86}	$13.8^{+4.9}_{-2.5}$	$16.5^{+60.9}_{-14.8}$	76^{+89}_{-52}	13.7/21 [8.4/15]	$0.67^{+0.36}_{-0.34}$	$37.7^{+1.4}_{-1.5}$	14.2/22 [8.8/16]
5	0.256 - 0.768	$5.4^{+0.7}_{-0.7}$	776^{+454}_{-236}	87^{+16}_{-11}	$11.7^{+0.4}_{-0.3}$	$88.4^{+16.5}_{-17.8}$	213^{+15}_{-20}	26.2/28	$0.36^{+0.12}_{-0.12}$	$37.6^{+0.5}_{-0.5}$	25.0/29
6	0.768 - 1.280	$7.3^{+0.5}_{-1.0}$	421^{+84}_{-58}	152^{+21}_{-21}	$14.0^{+0.8}_{-0.7}$	$27.5^{+11.6}_{-9.3}$	136^{+23}_{-23}	37.0/30	$0.04^{+0.11}_{-0.11}$	$37.6^{+0.6}_{-0.6}$	31.6/31
7	1.280 - 9.472 ^c	$7.7^{+0.6}_{-1.0}$	165^{+23}_{-60}	73^{+10}_{-25}	$14.5^{+5.2}_{-2.0}$	$3.7^{+7.8}_{-2.0}$	20^{+26}_{-11}	23.1/30	$0.70^{+0.46}_{-0.43}$	$32.9^{+1.1}_{-1.2}$	25.8/31
1 - 7 ^d	0.0 - 9.472 ^c	$6.4^{+0.4}_{-0.4}$	455^{+73}_{-55}	95^{+12}_{-11}	$12.4^{+0.4}_{-0.4}$	$43.5^{+8.8}_{-8.1}$	136^{+12}_{-14}	37.0/30	$0.20^{+0.08}_{-0.08}$	$35.7^{+0.3}_{-0.3}$	32.4/31

^a The luminosity of blackbody components calculated at $d=10$ kpc.

^b C-stat/dof for spectra 1 to 4; the quality of the corresponding χ^2 fit is given in square parentheses for reference.

^c The 2BB model radii and luminosities for spectra 7 and 1-7 are calculated using intervals 1.280–1.680 s and 0.0–1.680 s, respectively (see text).

^d The time-integrated spectrum.

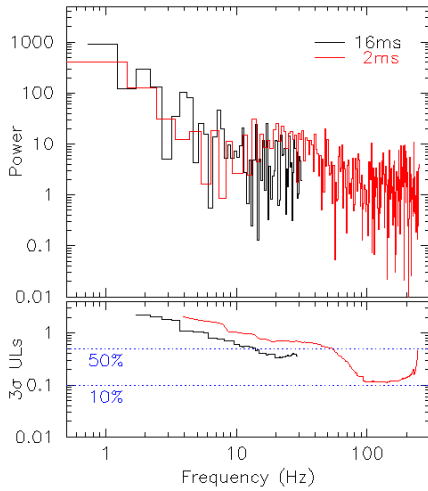


Figure 5. Power spectrum produced from the KW light curve in the G1+G2 energy range (upper panel). Curves representing the upper limits to the non-detection of pulsations are in the lower panel. The two horizontal dashed lines represent the 10 per cent and 50 per cent upper limits to the pulsed fraction. Lines of different colours correspond to the different time resolutions.

4 SEARCH FOR QPOS

We searched for pulsations in the 2 ms and 16 ms G1+G2 light curves by using the Fast Fourier Transform method without finding any statistically significant signal. Following the recipe described in [Israel & Stella \(1996\)](#) we derived upper limits to the pulsed fraction at a 3σ confidence level of >50 per cent for frequencies in the 5–60 Hz range and 10–30 per cent between 60 and 250 Hz (see Fig. 5).

When compared to the QPO amplitudes detected in tails of GFs these limits are not very strict. The main QPOs in the GFs of SGR 1806-20 and SGR 1900+14 ([Israel et al. 2005](#); [Strohmayer & Watts 2005](#)) have pulsed fractions of ~ 5 per cent at ~ 20 Hz, ~ 50 per cent at ~ 30 Hz, ~ 10 per cent at ~ 150 Hz and ~ 20 per cent at ~ 260 Hz. In all cases our inferred 3σ upper limits are well above or slightly above these values.

5 DISCUSSION

The rather long duration of the burst (longer than half the rotation period) along with the large measured energy fluence put it in the class of “intermediate” SGR flares, and this is the first one observed from SGR 1935+2154. The burst profile is rather structureless; it lacks a prominent initial peak seen in some SGR bursts of comparable (or longer) duration ([Mazets et al. 1999b](#); [Aptekar et al. 2001](#); [Olive et al. 2004](#)) and does not show any evidence of an extended, modulated tail observed previously in a number of IFs (e.g. [Mereghetti et al. 2009](#); [Gögüş et al. 2011](#)). In the Type A/Type B morphological classification of magnetar bursts ([Woods et al. 2005](#)) such an event may be classified as Type A.

A spectral model that best describes the SGR 1935+2154 burst spectra cannot be selected unambiguously from our analysis. Of the four spectral functions tested, only two simple models, OTTB and single BB, can be rejected on statistical grounds while two more complex models, CPL and 2BB, fit the TI spectrum and all seven TR spectra reasonably well and neither of them may be ruled out by our observations. The main reason behind this is that, given the observed count statistics and the derived model parameters, the CPL and 2BB spectra can successfully mimic each other in the relatively hard (20–250 keV) KW spectral band. Similar results were obtained in the *Fermi*/GBM studies of SGR J0501+4516 and SGR J1550-5418 bursts in the softer 8–200 keV band ([Lin et al. 2011](#); [van der Horst et al. 2012](#)). However, with the use of the *Swift*/XRT 0.5–10 keV data, it was shown that the broadband (0.5–200 keV) spectra of SGR J1550-5418 bursts observed simultaneously with GBM and XRT are better described with two blackbody function than with the Comptonized (CPL) model ([Lin et al. 2012](#)). Thus, broadband studies of SGR 1935+2154 are needed to reach more conclusive results on its spectral behaviour.

The CPL model is intended to approximate the unsaturated Comptonization spectrum, and its implications in the context of magnetars are presented in detail in [Lin et al. \(2011\)](#). The E_p value we obtained from the CPL model fits, $E_p \sim 30$ –40 keV, is typical for SGR bursts (see, e.g., [Aptekar et al. 2009](#); [Lin et al. 2011](#); [Ferochi et al. 2004](#)). The OTTB function, which is often considered for SGR spec-

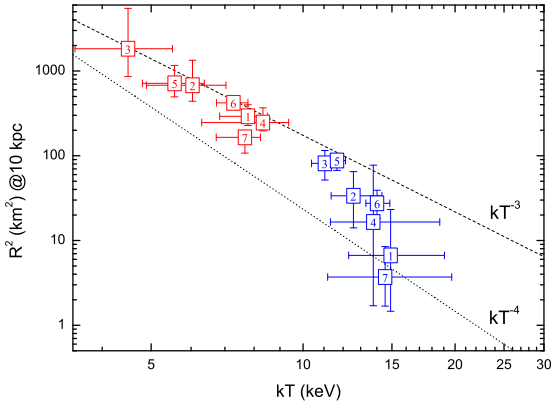


Figure 6. Squares of the radii of the emitting areas as a function of their temperatures. The soft BB component is shown in red and the hard BB in blue. Numbers correspond to the spectral intervals. We also plot the $R^2 \propto kT^{-3}$ and $R^2 \propto kT^{-4}$ power laws (the latter corresponds to the relation for a pure BB with $L = 3 \times 10^{40}$ erg s $^{-1}$).

tra above 15 keV (e.g. [Aptekar et al. 2001](#)), does not fit the TI spectrum nor any individual burst spectra after $T_0 + 0.128$ s ($\chi^2/\text{dof} > 2$). Accordingly, the hard photon index obtained from the CPL fits ($\alpha \gtrsim -0.3$) is inconsistent with the OTTB slope of -1 . Our result for the CPL photon index is close to those reported for SGR 0501+4516 ([Aptekar et al. 2009](#); [Lin et al. 2011](#)) and SGR 1900+14 ([Feroci et al. 2004](#)), and is significantly harder than the OTTB-like slope initially derived for SGR J1550-5418 from the GBM observations by [van der Horst et al. \(2012\)](#). It was shown by [Lin et al. \(2012\)](#) that the broadband XRT+GBM spectra of SGR J1550-5418 bursts better constrain the photon indices, which become harder than the ones derived from the GBM-only data. They also noticed that a classical, unsaturated Comptonization model has difficulty in generating spectral slopes with $\alpha > -1$ and that such flat spectra might naturally be expected to exhibit a more truly thermalized character. A generalized Comptonization model (CompTT; [Titarchuk 1994](#)), where soft photons are upscattered in a hot plasma taking into account relativistic effects, have been shown to be similar to the 2BB performance in the broadband study of SGR 1900+14 bursts with *Swift*/BAT and XRT ([Israel et al. 2008](#)). We fitted this model (implemented as CompTT in XSPEC) to the SGR 1935+2154 spectra with good count statistics and obtained χ^2 values between those of CPL and 2BB. This demonstrates the good statistical performance of CompTT on the IF spectra, but a more detailed discussion of this model is beyond the scope of this paper.

The most plausible interpretation of the 2BB model is the emission originating from two hot spots with different temperatures near or on the neutron star surface or in its magnetosphere where local thermodynamic equilibria are achieved. For the TI spectrum, the temperatures and radii we obtained for the 2BB model are typical of that for other SGR sources: $kT_1 \sim 3\text{--}7$ keV, $R_1 \sim 10\text{--}30$ km and $kT_2 \sim 10\text{--}20$ keV, $R_2 \sim 4$ km; see [Nakagawa et al. \(2007\)](#) for SGR 1806-20 and SGR 1900+14, [Esposito et al. \(2008\)](#) for

SGR 1627-41, [van der Horst et al. \(2012\)](#) for SGR J1550-5418, and [Lin et al. \(2011\)](#) for SGR J0501+4516. Specifically, the derived 2BB model parameters are in reasonable agreement with the results reported previously for intermediate bursts: $kT_1 \sim 4.8$ keV, $R_1 \sim 30$ km and $kT_2 \sim 9.0$ keV, $R_2 \sim 5.7$ km ([Israel et al. 2008](#); [Olive et al. 2004](#)). Finally, the spectral parameters we measured for the IF are consistent with those obtained from observations of much weaker and shorter bursts from SGR 1935+2154 in 2014 July ([Lien et al. 2014](#)) and in 2015 February ([Burns & Younes 2015](#)). This suggests that similar physical processes may be responsible for the IF and the weak bursts despite orders of magnitude difference in the amount of energy released.

Using the 2BB fits described in Section 3, we calculated the soft and hard BB luminosities for each of the seven TR spectra (Tab. 1). All the derived bolometric luminosities are over 10^{40} erg s $^{-1}$, and hence there is a slight hint of the saturation effect of the low- kT BB luminosity as previously noted for SGR 1900+14 ([Israel et al. 2008](#)). In order to further investigate this trend, we studied the R^2 versus kT distribution (see Fig. 6). The sharp edge in the distribution of the data described by the $R^2 \propto kT^{-3}$ relation indicates the presence of the saturation. So we can use the magnetic Eddington luminosity formula derived in [Paczynski \(1992\)](#):

$$L_{\text{Edd,B}} \approx 2 \times 10^{40} \left(\frac{B}{B_{\text{QED}}} \right)^{4/3} \left(\frac{R}{R_{\text{NS}}} \right)^{2/3}, \quad (1)$$

where B is the magnetic field at the radius R , $B_{\text{QED}} \simeq 4.4 \times 10^{13}$ G is magnetic field critical value and R_{NS} is the neutron star radius for which we assume a typical value of 10 km. It can be rewritten in terms of the distance d and peak flux F_{max} as

$$\left(\frac{d}{\text{kpc}} \right) \simeq 0.4 \times \left(\frac{F_{\text{max}}}{10^{-5} \text{ erg cm}^{-2} \text{ s}^{-1}} \right)^{-1/2} \left(\frac{kT_{\text{break}}}{\text{keV}} \right)^{5/4} \times \left(\frac{B_{\text{surf}}}{10^{14} \text{ G}} \right)^{1/4} \left(\frac{R_{\text{NS}}}{10 \text{ km}} \right)^{5/8}, \quad (2)$$

where kT_{break} is the energy at which the data in the R^2 versus kT distribution start departing from the relation kT^{-3} . Now we can estimate an approximate value for the source distance by using the saturated flux recorded for the source and the magnetic field strength inferred by timing analysis. For the surface magnetic field B_{surf} we use a dipolar magnetic field value of $\sim 2.2 \times 10^{14}$ G inferred for SGR 1935+2154 by [Israel et al. \(2016\)](#) from *Chandra* observations. With the value of kT_{break} for this burst lying in the 12–15 keV range we derive a distance of 7.4–9.8 kpc. However, given that we have seen only one bright IF from this source, we cannot be sure that the luminosity in the April 12 burst is close to the maximum observable from SGR 1935+2154 and a brighter burst would situate the source closer to us. So, in this work, we estimate the SGR 1935+2154 distance to be < 10.0 kpc, in agreement with that of the Galactic supernova remnant G57.2+0.8. Assuming isotropic emission at 9.1 kpc, the total bolometric energy release in the flare is $\sim 3.3 \times 10^{41}$ erg and the bolometric peak luminosity is $\sim 3.0 \times 10^{41}$ erg s $^{-1}$; both of them lie close to the lower end of the IF range.

ACKNOWLEDGEMENTS

We would like to thank the anonymous referee for providing comments that helped to improve the paper. We are grateful to W. Boynton, C. Fellows, K. Harshman, A. S. Kozyrev, M. L. Litvak, A. B. Sanin, A. Rau and A. von Kienlin for the use of their data in the IPN triangulation. DDF acknowledges support from RFBR grant 15-02-00532a. KH acknowledges support for MESSENGER data analysis from NASA Grant NNX07AR71G.

REFERENCES

- Andersson N., Kokkotas K. D., 1996, *Phys. Rev. Lett.*, **77**, 4134
 Aptekar R. L., et al., 1995, *Space Sci. Rev.*, **71**, 265
 Aptekar R. L., Frederiks D. D., Golenetskii S. V., Il'inskii V. N., Mazets E. P., Pal'shin V. D., Butterworth P. S., Cline T. L., 2001, *ApJS*, **137**, 227
 Aptekar R. L., Cline T. L., Frederiks D. D., Golenetskii S. V., Mazets E. P., Pal'shin V. D., 2009, *ApJ*, **698**, L82
 Arnaud K. A., 1996, in Jacoby G. H., Barnes J., eds, *Astronomical Society of the Pacific Conference Series Vol. 101, Astronomical Data Analysis Software and Systems V*. p. 17
 Burns E., Younes G., 2015, *GCN Circular* 17496
 Cummings J., Barthelmy S., Chester M., Page K., 2014, *ATel* #6294
 Doneva D. D., Gaertig E., Kokkotas K. D., Krüger C., 2013, *Phys. Rev. D*, **88**, 044052
 Esposito P., et al., 2008, *MNRAS*, **390**, L34
 Feroci M., et al., 2003, *ApJ*, **596**, 470
 Feroci M., Caliendo G. A., Massaro E., Mereghetti S., Woods P. M., 2004, *ApJ*, **612**, 408
 Frederiks D. D., et al., 2013, *ApJ*, **779**, 151
 Gaensler B., 2014, *GCN Circular* 16533
 Gold R. E., et al., 2001, *Planet. Space Sci.*, **49**, 1467
 Golenetskii S. V., Ilinskii V. N., Mazets E. P., 1984, *Nature*, **307**, 41
 Golenetskii S., et al., 2015, *GCN Circular* 17699
 Göğüş E., et al., 2011, *ApJ*, **740**, 55
 Huppenkothen D., et al., 2014a, *ApJ*, **787**, 128
 Huppenkothen D., Heil L. M., Watts A. L., Göğüş E., 2014b, *ApJ*, **795**, 114
 Hurley K., et al., 2005, *Nature*, **434**, 1098
 Hurley K., et al., 2006, *ApJS*, **164**, 124
 Israel G. L., Stella L., 1996, *ApJ*, **468**, 369
 Israel G. L., et al., 2005, *ApJ*, **628**, L53
 Israel G. L., et al., 2008, *ApJ*, **685**, 1114
 Israel G., Rea N., Zelati F., Esposito P., Burgay M., Mereghetti S., Possenti A., Tiengo A., 2014, *ATel* #6370
 Israel G. L., et al., 2016, *MNRAS*, **457**, 3448
 Lien A. Y., et al., 2014, *GRB Coordinates Network*, **16522**, 1
 Lin L., et al., 2011, *ApJ*, **739**, 87
 Lin L., et al., 2012, *ApJ*, **756**, 54
 Mazets E. P., Golenetskii S. V., 1981, *Ap&SS*, **75**, 47
 Mazets E. P., Cline T. L., Aptekar R. L., Butterworth P. S., Frederiks D. D., Golenetskii S. V., Il'inskii V. N., Pal'shin V. D., 1999a, *Astronomy Letters*, **25**, 635
 Mazets E. P., Aptekar R. L., Butterworth P. S., Cline T. L., Frederiks D. D., Golenetskii S. V., Hurley K., Il'inskii V. N., 1999b, *ApJ*, **519**, L151
 Mereghetti S., 2013, *Brazilian Journal of Physics*, **43**, 356
 Mereghetti S., Götz D., von Kienlin A., Rau A., Lichti G., Weidenspointner G., Jean P., 2005, *ApJ*, **624**, L105
 Mereghetti S., et al., 2009, *ApJ*, **696**, L74
 Nakagawa Y. E., et al., 2007, *PASJ*, **59**, 653
 Olausen S. A., Kaspi V. M., 2014, *ApJS*, **212**, 6
 Olive J.-F., et al., 2004, *ApJ*, **616**, 1148
 Paczynski B., 1992, *Acta Astron.*, **42**, 145
 Pavlović M. Z., Urošević D., Vukotić B., Arbutina B., Göker Ü. D., 2013, *ApJS*, **204**, 4
 Protassov R., van Dyk D. A., Connors A., Kashyap V. L., Siemiginowska A., 2002, *ApJ*, **571**, 545
 Rau A., Kienlin A. V., Hurley K., Lichti G. G., 2005, *A&A*, **438**, 1175
 Stamatikos M., Malesani D., Page K. L., Sakamoto T., 2014, *GCN Circular* 16520
 Strohmayer T. E., Watts A. L., 2005, *AAS*, **37**, p 1497
 Titarchuk L., 1994, *ApJ*, **434**, 570
 Woods P. M., et al., 2005, *ApJ*, **629**, 985
 van der Horst A. J., et al., 2012, *ApJ*, **749**, 122

This paper has been typeset from a $\text{\TeX}/\text{\LaTeX}$ file prepared by the author.